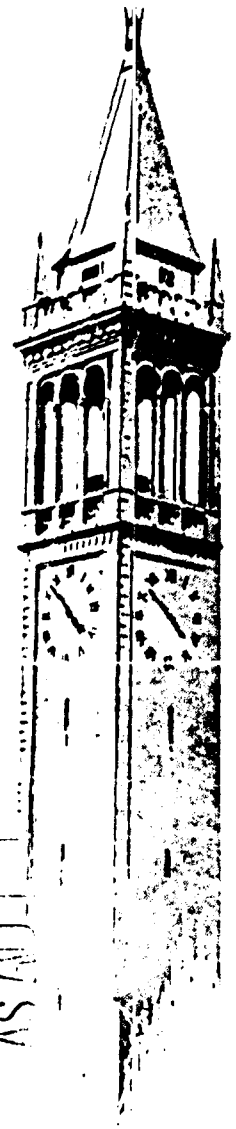

MEASUREMENT OF SHOCK WAVE THICKNESS BY THE ELECTRON BEAM FLUORESCENCE METHOD

by

F. Robben
L. Talbot

Report No. AS-65-4
Contract Nonr-222(45) & Grant AFOSR-538-65
May 1965

INSTITUTE OF ENGINEERING RESEARCH

UNIVERSITY OF CALIFORNIA
Berkeley, California

CONTRACTS
Nonr-222(45)
AFOSR 538-65
REPORT NO. AS-65-4
MAY 1965

SPONSORED BY
OFFICE OF NAVAL RESEARCH
AIR FORCE OFFICE OF SCIENTIFIC RESEARCH
ADVANCED RESEARCH PROJECTS AGENCY

MEASUREMENT OF SHOCK WAVE THICKNESS BY THE ELECTRON BEAM FLUORESCENCE METHOD

by

F. Robben
L. Talbot

FACULTY INVESTIGATORS:
S. A. SCHAAF, PROFESSOR OF ENGINEERING SCIENCES
L. TALBOT, PROFESSOR OF AERONAUTICAL SCIENCES
G. J. MASLACH, PROFESSOR OF AERONAUTICAL ENGINEERING
F. C. HURLBUT, ASSOCIATE PROFESSOR OF AERONAUTICAL SCIENCES
F. S. SHERMAN, ASSOCIATE PROFESSOR OF AERONAUTICAL SCIENCES
D. R. WILLIS, ASSISTANT PROFESSOR OF AERONAUTICAL SCIENCES
S. A. BERGER, ASSISTANT PROFESSOR OF AERONAUTICAL SCIENCES

ABSTRACT

Shock wave thicknesses and density ratios have been measured in helium, argon and nitrogen by means of the electron beam fluorescence method, over the range $1.5 < M < 17.4$, in a low density wind tunnel. The shock thicknesses in argon and helium agreed well with Mott-Smith theory at the higher Mach numbers, and were between Navier-Stokes and Mott-Smith theory at the lowest Mach number. In nitrogen, the measured shock thicknesses were considerably greater than the predictions of Navier-Stokes theory.

Measured density ratios across the shock wave were in good agreement with theory, in the lower density flows. Poorer agreement was found at higher flow densities, leading to estimates of upper bounds for the range of linear variation of fluorescence intensity with gas density. Measured density ratios for shocks produced in divergent free-jet flows were found to be in better agreement with theory after a viscous curvature correction was applied.

1.0 INTRODUCTION

Several different techniques have been employed successfully to measure the thickness and internal structure of shock waves. The earliest determinations of shock wave thickness were made by means of the optical reflectivity technique (see Linzer and Hornig,[1] and the references cited therein). At about the same time the optical reflectivity technique was being perfected, measurements of the internal structure of shock waves were carried out by means of free-molecule probes.[2,3] Results obtained by these two techniques and comparisons with theory are discussed in the survey papers by Sherman and Talbot[4] and Talbot.[5]

The most recent experimental studies of shock wave structure have been by electron beam techniques. The idea of using an electron beam dates back at least to the work of Ballard and Venable,[6] who observed the change in transmission of an electron beam directed across a shock tube, due to the passage of a shock wave. Only a few data points were obtained, however, and these were subject to rather large experimental uncertainty. Recently Russell[7] has succeeded in improving the accuracy of the method considerably, mainly by the use of a large-diameter low-density shock tube, and has reported new data on the density thickness of argon shock waves. Similar work has been reported by Schultz-Grunow and Frohn.[8]

Another method of using an electron beam for probing shock waves has been developed by Camac,[9] who observes the electrons scattered out of the beam by collisions, rather than the portion of the beam which is transmitted unattenuated across the shock tube. With this method, Camac has obtained shock thickness data for argon, nitrogen and carbon dioxide. His argon results are in reasonably good agreement with those of Russell.

Still another technique involving the use of an electron beam is available for studying shock wave structure. This is the electron beam fluorescence

fairly comprehensive picture of the problem, especially for monatomic gases. Our main purpose in carrying out the present series of experiments has in fact been to use the shock wave flow as a testing ground for assessing the accuracy and limitations of the electron-beam-fluorescence technique, although of course in the process of so doing we have attempted to extend the available data and obtain certain new results.

2.0 DESCRIPTION OF THE METHOD

2.1 Equipment

The theory underlying the electron-beam fluorescence technique is described in the papers by Muntz[11] and Muntz and Marsden.[12] We shall not go into an extended description here, and we refer the reader to these papers for details.

The experimental arrangement used in the present tests is shown in Fig. 1. The electron beam source is a commercial Alloyd electron-beam welder, rated at 30 kV and 150 mA. (In the tests, beam currents in the range 1.5 - 10 mA were used, at 30 kV.) Downstream of the exit orifice of the beam chamber a magnetic X-Y deflection coil system, also manufactured by Alloyd, was used to direct the beam into the desired trajectory. The wind tunnel static pressure was typically in the 10^{-1} Torr range, and a 3-inch oil diffusion pump attached to the beam chamber was adequate to keep the beam chamber pressure below 2×10^{-4} Torr when a 0.040 inch diameter exit orifice was used.

Shock waves were produced in the flow by means of a shock-holder. A water-cooled "choker" device downstream of the shock-holder was positioned so that the shock wave stood slightly ahead of the shock-holder. Slots about 1/4 inch long were cut in the sides of the shock-holder, so that the flow could be observed some distance downstream of the entrance. The shock waves could be observed visually in the darkened tunnel, because the primary electron beam,

together with the "halo" around it (presumably produced by secondary electrons), illuminated a substantial area of the shock wave. All of the shock waves studied appeared to be quite plane, although no precise measurements of shock curvature were attempted. (Some discussion of shock curvature effects is given later in this report.) The shock-holder choker had a 0.080 inch diameter collimating hole, through which the electron beam passed, at a slight angle to the axis of the flow, and upstream of the shock wave the beam was collected by a water-cooled cup. The current to this cup was used in a feedback loop to regulate the voltage on the bias grid of the electron gun, in order to maintain a constant beam current.

The optical detection system is also illustrated schematically in Fig. 1. The entrance slit of a Jarrell-Ash 3.4 meter Ebert spectrograph was imaged at approximately unity magnification perpendicular to the electron beam, by a 48 inch focal length spherical mirror and a plane mirror, as shown. The slit image was scanned along the electron beam by rotating the plane mirror, and the output of a 10-turn potentiometer linked to the motor-driven micrometer drive of the plane mirror was coupled to the X-axis of an X-Y recorder. The radiation from the beam was detected by an uncooled 1P-21 photomultiplier tube, whose output was amplified by a Model 600A Keithley electrometer and fed to the Y-axis of the recorder. A stack of ten 67.5-Volt batteries was used to power the photomultiplier. While batteries probably have no particular advantage over a regulated power supply used with a voltage divider, they have proven to be stable, trouble free, and inexpensive. In almost all cases, the photomultiplier was placed directly behind the 50 micron entrance slit, so that the spectrometer was not used as such. The only spectral resolution of the radiation in the actual shock wave measurements was that afforded by a Corning 7-59 blue filter placed ahead of the entrance slit in the argon and nitrogen measurements. The filter was not used for the helium measurements. However, spectral analyses

of the radiation were carried out under both static and flow conditions. The principal source of the observed radiation in nitrogen was found to be the 3914 Å, (0,0) band of the first negative system of N_2^+. In argon, the radiation comes principally from lines of AI and AII between 3000 and 4000 Å, although there are a number of lines in the red which were excluded by the filter. In helium the 5015 Å 3^1P and 4471 Å 4^3D lines are responsible for most of the radiation, the latter line having about 5% the intensity of the former.

2.2 Spatial Resolution

The resolution of the optical system was estimated to be about 0.002 inch, measured along the beam axis, when a 0.050 mm entrance slit was used. This estimate was arrived at by scanning the slit image across a knife-edge located within the wind tunnel. The knife-edge was illuminated from behind, and the resolution was taken arbitrarily to be the distance of slit-image travel corresponding to the increase from 10% to 90% of the total light intensity observed by the photomultiplier as the slit-image traversed the occulting knife-edge.

An additional factor contributing to the overall resolution is the convection downstream of the radiating atoms and molecules. Some measurements of this effect were carried out by passing the electron beam vertically upward through a 0.018 inch semi-circular aperture (formed by half-plugging a 0.040 inch hole, with the flat edge of the aperture upstream) in a water-cooled wedge whose upper surface was aligned with the flow issuing from a Mach 4 nozzle. In the free stream region above the wedge shock wave, the beam fluorescence was scanned with and without flow, in order to determine the convective displacement of the radiation profile. This displacement x is approximately related to the lifetime τ of the excited state through $x = U\tau$, where U is the stream velocity. On the basis of the measured lifetime $\tau = 6.5 \times 10^{-8}$ sec of the (0,0) band of N_2^+ (see Ref. 15) the

displacement x in N_2 should have been about 0.0015 inch, whereas we observed $x \lesssim 0.002$ inch, with an experimental uncertainty of about 0.002 inch. No effort was made to determine the value more precisely. Similar small displacements were observed for the total radiation in argon (with blue filter), and the spectrally resolved 5015 Å 3^1P helium line. On the other hand, the spectrally-resolved radiation from the 4471 Å 4^3D helium line showed a significant ($x \approx 0.006$ inch) downstream shift.

The observed radiation profiles are shown in Figs. 2a and 2b. All represent data taken under flow conditions. It will be noted that the profiles obtained from argon, nitrogen and the 3^1P helium line are quite symmetrical. The 4^3D helium line, on the other hand, shows a pronounced asymmetry in the downstream direction. Of particular interest in these profiles is the intensity of the radiation in the "halo" surrounding the primary beam. This halo is believed to be due to excitation of the gas by secondary electrons resulting from ionizing collisions in the main beam, rather than to excitations by primary electrons which have undergone small-angle scattering out of the main beam. These secondary electrons will be of predominantly low energy, and in fact many of them may have insufficient energy to excite the observed N_2^+ radiation (see Muntz and Marsden,[12] and Mott and Massey[16]). Thus they will have a short mean free path, and would be expected to leave the primary beam by diffusive processes. The measurements of halo intensity shown seem to bear out these predictions. The magnitude of the halo in different gases would depend on the particular cross sections for the various important processes. The smallest relative halo intensity occurs in helium, with nitrogen only a little larger, while argon has a quite large halo intensity. Some measurements were made at different gas densities, covering about a factor of 3, and while in general the halo seemed to increase in relative intensity with gas density, the effect was not pronounced. The 4^3D line of helium shows somewhat more halo than the 3^1P line; however, the

4^3D line is only about 5% the intensity of the 3^1P. The measured shifts of these two lines of helium, and the halo intensity, are not understood, as they do not seem to correlate with the theoretical lifetimes[17] which have also been verified by experiment.[15] It must be remembered that a 537 Å resonance line also originates from the 3^1P level, and at the density and temperatures employed here this radiation will be strongly imprisoned, so that the lifetime of the 3^1P level should be given by decay through the 5015 Å radiation only.

The halo radiation is of concern in the shock wave measurements because one must look through the halo when observing the primary beam, even if the spectrograph slit height is chosen no larger than the primary beam diameter. In point of fact, it is preferable for the shock wave measurements to choose the slit height somewhat greater than the primary beam diameter, because in this way a small deviation from parallelism between the beam and the path followed by the slit image will not produce large errors; this procedure, however, increases the amount of halo radiation included with that of the main beam. Now, if the halo radiation intensity varies linearly with density, in the same way as does the primary beam, it should not present much of a problem in making shock wave density profile measurements. It appears from our data that the variation is approximately linear, but the evidence is not conclusive. But even if the halo intensity does vary linearly with density, it still appears to present a problem in making rotational temperature measurements in nitrogen. This is discussed in the companion reports.[13,14]

The combination of uncertainties due to the resolution of the optics and the downstream convection of excited species leads to the estimate of approximately 0.003 inch probable error in the location of a point in the flow. Since the shock waves reported here have maximum slope thicknesses greater than 0.030 inch, there should be no measurable distortion of either the shock wave profile or the maximum slope chickness, as pointed out by Russell.[7]

2.3 Free Stream Flows

Both contoured nozzles and free jet expansions[18,19] were used to produce the test flows. The gases were unheated, so that all stagnation temperatures were room temperature (~ 297°K). All flows were calibrated by measuring stagnation and impact pressures, and assuming isentropic flow. The impact pressures were corrected experimentally for viscous effects by testing a range of sizes of open-ended and source-shaped probes, and extrapolating to infinite probe diameter. In the case of the free jet flows, a correction was also made for shock-standoff distance. This correction is necessary because an axial gradient is present in the free jet flow, and the stream Mach number associated with the probe position is slightly higher than that of the probe shock wave.

Variation of the Mach number in the free jet tests was achieved by keeping the shock-holder at a fixed position (about 6 inches downstream of the orifice plates) and changing the diameter of the sonic orifice. This procedure was more convenient than varying the distance between the shockholder and a fixed-diameter orifice. Orifice diameters of 1/4, 1/2, 1 and 4 inches were used. The three smallest orifice plates were machined from 1/4 inch thick aluminum plate, and the orifices had 1/4 inch radius fillets to provide a smooth transition from the upstream surface of the plate to the exit of the orifice. The 4-inch orifice was cut into a 0.125"plate, and the edges were left sharp. At each flow Mach number, for both the orifices and the nozzles, the stagnation pressure p_o and hence the free stream density was varied by a factor of 4 or more. This variation produced negligible changes in M_1 for the orifice flows, but it did change the exit Mach numbers in the nozzle flows because of the change in nozzle boundary layer thickness.

The No. 4, Mach 3 nozzle is an axisymmetric contoured nozzle which was fabricated a number of years ago. Although it was not one of the more successful nozzles made for the low density tunnel, in that it has some

pronounced flow non-uniformities, it was used in the present tests because the data taken near Mach 3 using the 4 inch sonic orifice was not felt to be as reliable as the other measurements. It was thought that there may be some viscous effects in the flow produced with this large orifice. Unfortunately, the lowest densities at which the Mach 3 nozzle could be operated were quite high, compared to the rest of the flows, and it appeared that the fluorescence technique develops some non-linearities at these densities. The No. 11, Mach 1.5 nozzle is the monatomic gas nozzle designed by Talbot and Sherman for their earlier shock wave studies, and it produces quite uniform flow. The data obtained in the Mach 3 nozzle are considered to be subject to more uncertainty than that obtained in the Mach 1.5 nozzle.

Table I gives a list of flow conditions representative of those used in the present tests. Also listed in the Table are values of the length $L^* = \mu(T^*)/\rho u$ which for reasons discussed later was chosen as the normalizing length for the measured shock wave thicknesses. ρu is the mass flux per unit area in the stream, which is constant through a normal shock wave, and $\mu(T^*)$ is the viscosity evaluated at the sonic temperature $T^* = 2T_o/(\gamma+1)$. Of course T^* is not the temperature which actually exists at the sonic point within a shock wave, because the flow in the interior of a shock wave is generally not locally adiabatic, but it is nevertheless a useful reference temperature.

3.0 RESULTS

3.1 Density Calibrations

Preliminary to the shock wave measurements, some static (no-flow) measurements were made in the wind tunnel of the light intensity emitted from the beam as a function of gas density. It is of course necessary to make such measurements at constant beam current, and it was found that an acceptable measurement of beam current could be made only if the beam was directed into

a shielded cup. This cup consisted of a closed water-cooled outer copper cylinder, within which was a slightly smaller copper cylinder, electrically isolated but conduction-cooled by boron nitride spacers The beam was accepted through an aperture at one end of the cup consisting of a 0.102 inch diameter hole in the outer cylinder, followed by a 0.110 inch hole in the inner cylinder. The outer cylinder was held at ground potential, while the inner cylinder was connected to the current metering circuit. The object of this arrangement was to insure that the measured current was due only to the primary high energy electrons.

The light intensity emitted from the beam, at a point about 1/2 inch ahead of the beam cup, was measured as a function of gas density, with the beam current held constant. The data indicated a reasonably linear variation of light intensity with gas density, although the density range which could be covered was not very large. (In order to avoid spurious signals from the afterglow produced by long-lived metastables, a small flow was maintained by the mechanical roughing pump on the tunnel, and the range over which this pump could operate fixed the density range of the calibration.) However, an accurate calibration was not required for the shock wave measurements, because the density ratio across a shock wave is known, and the ability of the electron beam technique to measure this ratio accurately at different ambient densities is in fact a quite satisfactory test of the linearity of the measurement.

An interesting by-product of the static calibrations was the observation that although there was considerable radiation in the beam halo, the current in the halo was essentially zero. This observation was made by traversing the entrance orifice of the shielded cup across the halo region. The absence of current in the halo region is quite conclusive evidence for the interpretation that the halo is produced by secondary electrons rather

than by primary electrons which have undergone small-angle scattering out of the main beam

3.2 Shock Wave Thicknesses

Figures 3a - 3d show some typical shock profiles traced directly from the X-Y recorder plots. The maximum-slope thickness δ_m was obtained by drawing, by eye, a straight line through the maximum slope point of the profile and measuring the distance between the intersections of this line with the extrapolations of the upstream and downstream flow regions. The density ratio ρ_2/ρ_1 across the shock was determined by extrapolating the upstream and downstream densities to the midpoint of the shock. It is believed that this procedure will account properly for any attenuation of the beam By moving the shock-holder choker downstream so that the shock was swallowed, measurement of the radiation intensity could be made in the free stream and compared with the known density. Some attenuation, of the order of 15% over the region traversed, was found. The attenuation depended on the gas density, being larger at higher gas densities. It was also found to depend on the alignment of the spectrometer slit image with the beam, and this would vary from time to time. After some initial attempts, it was decided not to correct the measurements for beam attenuation, principally because such corrections should not make any measurable differences in the maximum slope thicknesses, density ratios, or normalized shock profiles.

In the free jet flow, there is a small negative density gradient in the free stream ahead of the shock waves, although it is hardly discernable in Figs. 3b and 3d. A plane shock wave in a divergent stream is to first approximation equivalent to a curved shock wave in a parallel flow, and consequently in the free jet a small positive density gradient is produced behind a shock wave. The effect of shock curvature itself would be to add to this gradient, so that the total gradient observed is due to a combination of flow divergence

and shock curvature, plus any variation in radiation intensity associated with attenuation of the primary beam and halo. The argon trace shown in Fig. 3c is exhibited as an extreme case of downstream density gradient. Most argon traces did not exhibit this much downstream gradient, but in general the gradients behind the argon shocks were greater than those behind the nitrogen shocks, possibly due to the greater halo intensity surrounding the primary beam in argon. Gradient effects were much less behind the nozzle-produced shock waves, indicating that these shock waves were very nearly plane.

A very curious anomaly was observed in traces obtained for the free-jet helium shock waves, a typical one of which is shown in Fig. 3d. In all of the free-jet measurements, a "dip" in radiation intensity was found in the upstream tail of the shock wave. Whether or not this dip corresponds to a dip in fluid density is unknown. It was absent from the helium free-jet flow when the shock was swallowed by the shock-holder, and it was never observed in argon or nitrogen. It was likewise not observed in the helium shock waves produced in nozzle flows. The helium free-jet data for maximum-slope thickness are, because of this effect, subject to greater uncertainty than the argon and nitrogen data, and the situation is even less clear with regard to experimental density ratios for the helium free-jet data.

Reciprocal maximum slope thicknesses for argon and helium are plotted in Fig. 4, and for nitrogen in Fig. 5. Rather than use the upstream mean free path λ_1, we have chosen to normalize δ_m with the length $L^* = \mu^*/\rho u$ (thus forming a shock thickness Reynolds number $Re_\delta^* = \rho u\, \delta_m/\mu^*$). There are several reasons for this choice. The length L^*, being based on the viscosity at temperature T^*, is much more representative than λ_1 of the conditions in the middle of the shock wave where δ_m is measured. Another advantage which accrues from the use of L^* is that theoretical predictions show that L^*/δ_m is quite insensitive to the viscosity-temperature law, and also that

L^*/δ_m asymptotes to a constant value as $M_1 \to \infty$. Finally, and most important, were we to use λ_1 as a reference length, we would be required to evaluate the viscosity μ_1 at very low temperatures, where it is not at all well known. In Fig. 4, the free jet data for all stream densities at a given Mach number have been averaged and plotted as a single point. Error flags of ±7% would encompass all of the data at each Mach number. Individual points have been plotted for each stream density for the nozzle data, because the Mach number changed with stream density due to boundary layer effects as noted previously. No systematic trend of δ_m with ρ_1 was noted for the free jet experiments, indicating that in the range of densities covered by these experiments the response of the electron beam was linear with density. However, there appeared to be a trend of increasing δ_m with ρ_1 in the Mach 3 nozzle data. As discussed later on, this may be associated with nonlinearity of the fluorescence-density relationship.

Figure 4 also shows a comparison between our data and the predictions of the Navier-Stokes and Mott-Smith theories. The Navier-Stokes curve was taken from the paper of Schwartz and Hornig,[20] while the Mott-Smith curve is based on an average of the calculation of Muckenfuss[21] and of Schwartz and Hornig. The viscosities for the experimental points were calculated from the Bromley-Wilke[22] tables. It can be seen that our data agree quite well with the Mott-Smith theory, at the higher Mach numbers. At the lowest Mach numbers, our data fall between the Mott-Smith and Navier-Stokes theories, but a little closer to the former. Thus, the present low Mach number data represent shock thicknesses a little greater than those obtained previously by Talbot and Sherman.

For purposes of comparison we have in Fig. 4 plotted mean curves representing the argon data obtained by Russell and by Camac, as transposed to L^*/δ_m coordinates. The relationship between λ_1 and L^*, for Russell's data, is

$$\frac{L^*}{\lambda_1} = \left(\frac{6}{5\pi}\right)^{1/2} \left(\frac{\mu^*}{\mu_1}\right) \cdot \frac{1}{M_1} \tag{1}$$

while for Camac's data it is

$$\frac{L^*}{\lambda_1} = \frac{5}{16}\left(\frac{2\pi}{\gamma}\right)^{1/2} \left(\frac{\mu^*}{\mu_1}\right) \cdot \frac{1}{M_1} \tag{2}$$

Both formulas give essentially the same result for $\gamma = 5/3$. Since both of these investigators worked in shock tubes, with $T_1 \approx 300°K$, the corresponding values of T^* at large Mach numbers go as high as 5000°K, where viscosity data are subject to some uncertainty. For the high temperatures, we have used the argon viscosity values recommended by Amdur and Mason.[23] These values agree with those of Bromley and Wilke for $T \lesssim 1200°K$, but above this temperature the Amdur-Mason viscosities are substantially larger than the Bromley-Wilke values.

It can be seen that Russell's data and our own are in reasonably good agreement, while Camac's experiments yielded slightly thicker shock waves. Of course, a substantially different viscosity-temperature law could change the relative positions of the data. Although we have not shown the argon data obtained by Linzer and Hornig for the range $1.7 < M_1 < 5$, it may be noted that these also agree quite well with Mott-Smith theory. It is also of interest to note that Russell's data were in quite good agreement with shock wave thicknesses calculated by Chahine and Narasimha[24] and Anderson and Macomber[25] on the basis of the Bhatnagar-Gross-Krook model of the Boltzmann equation, after an ad hoc correction was applied to change from Prandtl No. = 1 to Prandtl No. = 2/3. Apparently, if this Prandtl Number correction can be accepted, there is little difference between the predictions of the B-G-K and the Mott-Smith theories.

Reciprocal shock thicknesses obtained in nitrogen are plotted in Fig. 5, following the same scheme as that used for the monatomic gas data. Also shown for comparison are the data of Linzer and Hornig and Camac. For Camac's data, T^* extends to values in excess of 4000°K, and we have evaluated $\mu(T^*)$ by both the Sutherland and the Bromley-Wilke formulas. The latter predicts somewhat larger viscosities for $T > 1000$°K. It can be seen that our results fall about where one might estimate an extrapolation of the Linzer-Hornig data to go. However, our measurements yielded shock waves considerably thinner than those observed by Camac. The lack of agreement between any of the data and Navier-Stokes theory with bulk viscosity $\kappa = 2\mu/3$ is evident. The Navier-Stokes curve was taken from Schwartz and Hornig. $\kappa = 2\mu/3$ is the value suggested by Sherman's[2] low Mach number measurements in air. The reason for the rather large discrepancy between Camac's data and our own is not clear. It would be difficult to assign the entire discrepancy to the uncertainty in $\mu(T^*)$ at high temperature, although this could be a contributory factor.

3.3 Shock Wave Density Ratios

A comparison between the experimental and theoretical density ratios in the form $\Delta \equiv (\rho_2/\rho_1)_{expt}/(\rho_2/\rho_1)_{theor}$ provides another test of the accuracy of the electron-beam fluorescence technique. In the Mach 1.5 nozzle, both the argon and nitrogen data corresponded to values in the range $\Delta = 1 \pm 0.02$, whereas the rather small amount of helium data obtained gave $\Delta = 0.94 \pm 0.03$. The agreement was poorer in the Mach 3 nozzle. Here the nitrogen data gave an average $\Delta = 0.95$, while the helium data gave $\Delta = 0.90$. The argon data, on the other hand, yielded $\Delta = 1.07$. We believe this poorer agreement in the Mach 3 nozzle is due principally to the failure of the linear relationship between beam intensity and gas density, and perhaps complicated by halo effects. The absolute free-stream gas density in the Mach 3 nozzle, at even the lowest

stagnation pressures in both argon and nitrogen, barely overlapped the highest free stream densities in the Mach 1.5 nozzle or free jet tests. If this explanation is correct, we can infer a rough upper bound estimate for the maximum density at which the fluorescence method can be used with confidence, at least for N_2 and argon. If we take conditions behind the shock wave as representative, then from both the nitrogen and the argon data this upper bound on density appears to be in the vicinity of 5×10^{-7} gm/cm^3. In round numbers, this density corresponds to pressures of about 0.25 Torr in argon, and 0.35 Torr in nitrogen at T = 300°K. Although the estimates are rough, they are not in conflict with Gadamer's data.

The halo radiation, especially in argon, may also contribute to the departures from $\Delta = 1$ in the Mach 3 nozzle. This effect is hard to estimate, because we do not have any reliable measurements on the intensity and extent of the halo radiation as a function of gas density. We did, however, make several scans of shock waves with the spectograph slit imaged so as to observe only the halo radiation above the primary beam. These shock profiles looked quite similar to those taken along the primary beam, but were slightly (about 10%) thicker. Perhaps this accounts for the fact that the Mach 3 data seem to be consistently a little farther below the Mott-Smith curve than the other data.

The experimental density ratios for the shock waves produced in the free jet flows can also be compared with the theoretical values of the modified Rankine-Hugoniot conditions for low-Reynolds-number spherical shock waves. The low-Reynolds-number correction to $(\rho_2/\rho_1)_{theor.}$ due to shock curvature was first examined by Germain and Giuraud.[26] Numerical results for a spherical shock wave have been calculated by Oberai.[27] Along the axis of symmetry (see Fig. 6), the corrected density ratio $(\rho_2/\rho_1)_{curv.}$ is according to Oberai related to the Rankine-Hugoniot value for plane shocks $(\rho_2/\rho_1)_{RH}$, by

$$(\rho_2/\rho_1)_{curv.} = (\rho_2/\rho_1)_{RH}\left(1 + \frac{\rho_{11} + \rho_{22}}{\rho_o}\ \epsilon\right) \qquad (3)$$

The factor $(\rho_{11} + \rho_{22})/\rho_o$ was found by Oberai to have the values -7.045 and -7.70 for $\gamma = 1.4$ and 1.67, respectively. The parameter ϵ is an inverse Reynolds number, defined by $\epsilon = \mu^*/\rho u\, R_b$, where R_b is the nose radius of the body producing the shock wave, but we have ignored the small difference between R_b and the shock wave radius R_s and have used instead $\epsilon = \mu^*/\rho u\, R_s$. The theory makes use of hypersonic approximations, and is therefore only applicable for, say, $M \gtrsim 3$.

For a curves shock wave in a slightly divergent source-flow, the effective shock radius one must use in evaluating ϵ is to first approximation

$$\bar{R}_s = \frac{R_o R_s}{R_o + R_s} \qquad (4)$$

where R_o is the radial distance from the shock to the source, as shown in Fig. 6. We assume, however, that our shock waves are plane, so we have taken $\bar{R}_s = R_o$. In Fig. 7 we have plotted values of $\Delta = (\rho_2/\rho_1)_{exp}/(\rho_2/\rho_1)_{RH}$ and $\Delta_{corr} = (\rho_2/\rho_1)_{exp}/(\rho_2/\rho_1)_{curv.}$ for our free-jet data. One observes that when the curvature correction is included, all the data can be represented by $\Delta_{corr} \cong 0.99 \pm 0.02$, whereas without the correction $\Delta \cong 0.97 \pm 0.02$. (We have corrected the low Mach number data as well, even though the theory is a hypersonic one.) Evidently, the curvature correction improves the agreement with theory to a point where the values of Δ obtained in the free-jet experiments agree very well with those obtained in the Mach 1.5 nozzle, and one may perhaps regard this as a tentative verification of the theory. Clearly, a more detailed investigation of this problem would be desirable and is within the capability of the electron-beam fluorescence method.

The density gradient behind the shock wave, due to flow divergence and shock curvature, can easily be calculated from elementary inviscid flow theory, if the shock wave is assumed to be vanishingly thin. One finds

$$\frac{d\rho_2}{dX} = \frac{2M_2^2\rho_2}{1 - M_2^2}\left[1 + \frac{2(M_1^2 - 1)}{2 + (\gamma-1)M_1^2}\right] \cdot \left(\frac{1}{R_o} + \frac{1}{R_s}\right) \qquad (5)$$

We compared this prediction with the experimental density gradients, assuming $R_s = \infty$, but the result was inconclusive. The experimental values were of the same order as the theoretical ones, but the scatter was as much as 100%. The scatter could be due to a variety of effects, such as noise in the traces, small deviations from planarity of some of the shock waves, and halo and scattering effects.

4.0 CONCLUSIONS

Shock wave thicknesses and density ratios were measured in helium, argon and nitrogen by means of the electron beam fluorescence method, over the Mach number range $1.5 < M < 17.4$, in a low density wind tunnel. Both contoured-nozzle and free-jet flows were used. The shock thicknesses in argon and helium agreed quite well with Mott-Smith theory at the higher Mach numbers, and were between Navier-Stokes and Mott-Smith theory at the lowest Mach number. For the higher Mach numbers good agreement was obtained with other measurements made by the electron beam attenuation,[7] electron beam scattering,[9] and optical reflectivity[1,20] methods. It is concluded that the electron beam fluoresence technique is at least as accurate as any of these other methods. In nitrogen, the measured shock thicknesses were considerably greater than the predictions of the Navier-Stokes theory. They agreed well with previous data obtained by the optical reflectivity method, but were considerably thinner than those measured by the electron beam scattering technique.

Measured density ratios across the shock waves in nitrogen and argon were in very good agreement with theory in a nominal Mach 1.5 nozzle. In a nominal Mach 3 nozzle, agreement was poorer, the reason apparently being a failure of the linear relationship between radiation intensity and gas density. This interpretation leads to rough upper bounds of $p = 0.25$ Torr and $p = 0.35$ Torr at room temperature for the pressures in argon and nitrogen, respectively, at which the fluorescence method can be used with confidence.

The density ratios across the shock waves in the divergent free-jet flows were subject to a viscous correction due to shock wave curvature. When a theoretical correction was applied, agreement between experiment and theory was very good, which can be interpreted as a tentative verification of the theory.

An anomalous dip was observed in radiation ahead of the helium shock waves produced in the free-jet flows. This dip was not observed in the helium shock waves produced in the nozzles, nor in any of the argon or nitrogen shock waves. The reason for the dip is not understood.

REFERENCES

1. M. Linzer and D. F. Hornig, Phys. Fluids 6, 1661 (1963).
2. F. S. Sherman, NACA TN-3298 (1955).
3. L. Talbot and F. S. Sherman, NASA Memo 12-14-58W (1959).
4. F. S. Sherman and L. Talbot, in Rarefied Gas Dynamics (L. Talbot, ed.), Academic Press, Inc., New York (1960), p. 161.
5. L. Talbot, ARS J. 32, 1009 (1962).
6. H. N. Ballard and D. Venable, Phys. Fluids 1, 225 (1958).
7. D. A. Russell, in Rarefied Gas Dynamics (J. H. deLeeuw, ed.), Academic Press, Inc., New York (1965). (In press)
8. F. Schultz-Grunow and A. Frohn, ibid.
9. M. Camac, ibid. See also AVCO Research Rept. 172 (1963).
10. B. W. Schumacher and E. O. Gadamer, Can. J. Phys. 36, 659 (1958). See also E. Gadamer, Univ. Toronto Inst. Aerophysics Rept. 83 (1962).
11. E. P Muntz, Phys. Fluids 5, 80 (1962).
12. E. P. Muntz and D. J. Marsden, in Rarefied Gas Dynamics (J. A. Laurmann, ed.), Academic Press, Inc., New York, Vol. II (1963), p. 495.
13. F. Robben and L. Talbot, Univ. of Calif. Rept. AS-65-5 (1965).
14. F. Robben and L. Talbot, Univ. of Calif. Rept. AS-65-6 (1965).
15. R. G. Bennett and F. W. Dalby, J. Chem. Phys. 31, 434 (1959).
16. N. F. Mott and H. S. W. Massey, Theory of Atomic Collisions, 2nd Edition, Oxford Univ. Press, London (1949), Chap. XI.
17. D. R. Bates and A. Damgaard, Phil. Trans. A242, 101 (1949).
18. F. S. Sherman, in Rarefied Gas Dynamics (J. A. Laurmann, ed.), Academic Press, Inc., New York, Vol. II (1963), p. 228.
19. H. Ashkenas and F. S. Sherman, in Rarefied Gas Dynamics (J. H. deLeeuw, ed.), Academic Press, Inc., New York (1965). (In press)

20. L. M. Schwartz and D. F. Hornig, Phys. Fluids 6, 1669 (1962).

21. C. Muckenfuss, Phys. Fluids 3, 321 (1960); Phys. Fluids 5, 1325 (1962).

22. L. A. Bromley and C. R. Wilke, Ind. Eng. Chem. 43, 1641 (1951).

23. I. Amdur and E. A. Mason, Phys. Fluids 1, 370 (1958).

24. M. Chahine and R. Narasimha, in Rarefied Gas Dynamics (J. H. deLeeuw, ed.), Academic Press, Inc., New York (1965). (In press)

25. D. G. Anderson and H. K. Macomber, ibid.

26. P. Germain and J. P. Giuraud, O.N.E.R.A. Rept. No. 105 (1962).

27. M. M. Oberai, J. de Mechanique 3, 173 (1964).

TABLE I. REPRESENTATIVE FLOW CONDITIONS

	ARGON			HELIUM			NITROGEN		
	M	p_o (Torr)	L^* (cm)	M	p_o (Torr)	L^* (cm)	M	p_o (Torr)	L^* (cm)
#11 Nozzle	1.68	0.178	0.0313	1.68	0.362	0.0476	1.69	0 187	0.0349
"	1.78	0.356	0.0167				1.72	0.254	0.0262
"	1.69	0.238	0.0263				1.58	0.145	0.0426
"	1.59	0.121	0.0440				1.77	0.370	0.0188
#4 Nozzle	2.50	0.871	0.0109	2.80	1.94	0.0182	2.66	0.931	0.0162
"	2.73	1.46	0.0760	2.94	3.41	0.0112	2.79	1.27	0.0135
"	2.59	0.759	0.0133				2.91	1.78	0.0108
"	2.62	1.04	0.0101						
"	2.87	1.49	0.00818						
4" D Free Jet	3.42	0.697	0.0260	3.42	0.528	0.0988	3.10	0.356	0.0643
"	3.42	0.411	0.0443	3.42	0.870	0.0640	3.10	0.723	0.0324
"	3.42	0.270	0.0620	3.42	1.49	0.0366	3.10	1.12	0.0206
"	3.42	1.11	0.0172				3.10	2.31	0.0101
"	3.42	2.17	0.00840						
1" D Free Jet	10.7	6.00	0.0603	10.7	7.82	0.138	6.87	5.30	0.0851
"	10.7	9.88	0.0366	10.7	12.4	0.0874	6.87	10.8	0.0432
"	10.7	15.2	0.0236	10.7	21.9	0.0493	6.87	25.3	0.0187
"	10.7	23.5	0.0153						
$\frac{1}{2}$" D Free Jet	17.4	15.4	0.0909	17.4	30.7	0.144	9.40	20.7	0.0963
"	17.4	23.5	0.0628	17.4	50.7	0.0880	9.40	41.9	0.0481
"	17.4	40.2	0.0368	17.4	93.5	0.0494	9.40	65.3	0.0308
"	17.4	60.9	0.0241				9.40	132.	0.0155
"	17.4	93.5	0.0159						
$\frac{1}{4}$" D Free Jet							12.7	81.2	0.0995
"							12.7	168.	0.0498
"							12.7	259.	0.0318

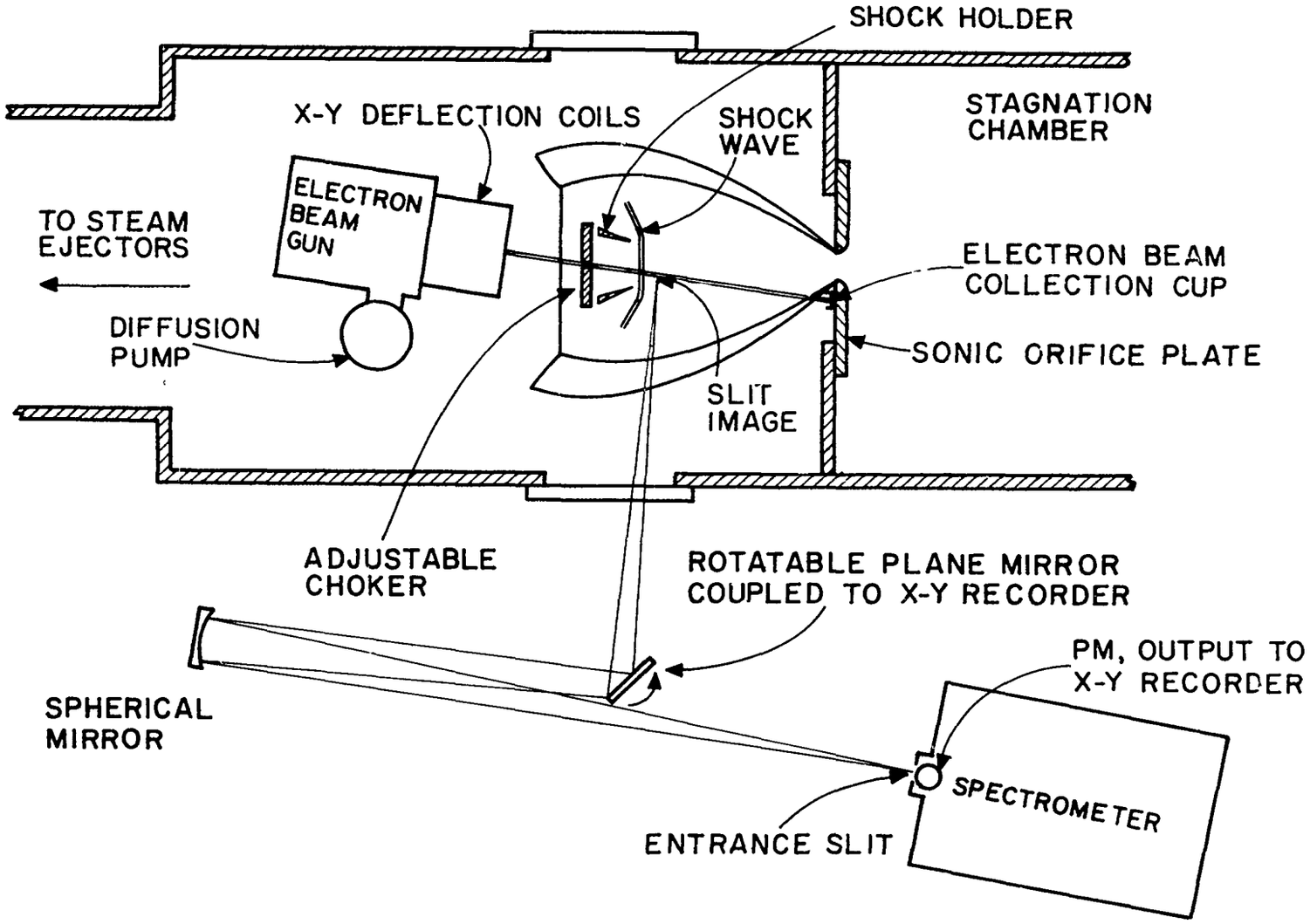

HYD-8359

FIG. 1. SCHEMATIC OF EQUIPMENT FOR SHOCK WAVE MEASUREMENTS IN FREE JET

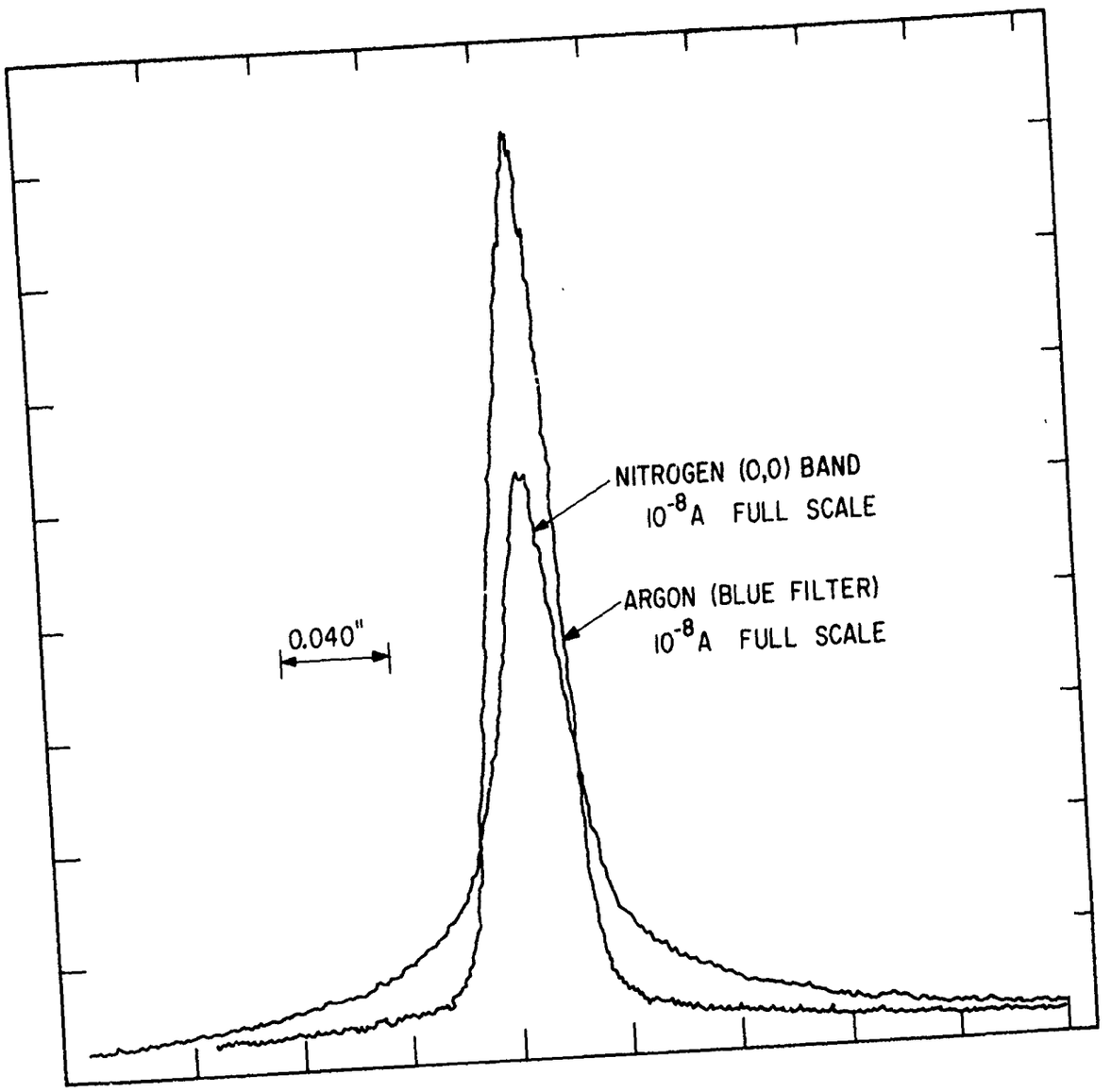

FIG. 2a. BEAM RADIATION PROFILES IN NITROGEN AND ARGON

Nitrogen: Mach 3.8, 30 kV beam at 1.5 mA, 10^{-8} A full scale on chart

Static density equivalent p = 0.30 Torr at 297°K

Argon: Mach 4.12, 30 kV beam at 1.0 mA, 10^{-8} full scale

Static density equivalent 0.34 Torr at 298°K

HYD-8360

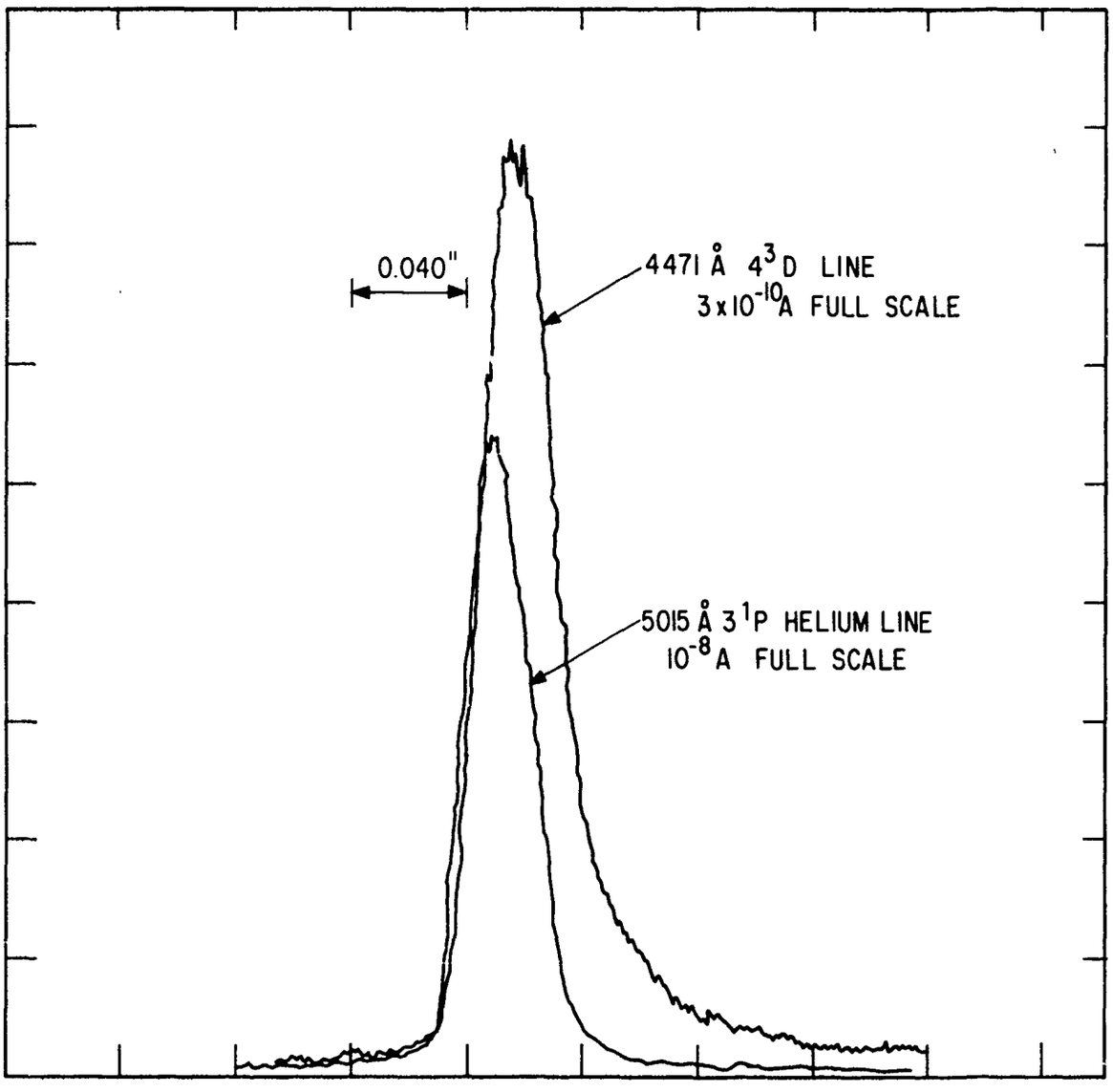

FIG. 2b. BEAM RADIATION PROFILES IN HELIUM

Mach 4.17, 30 kV beam at 2.0 mA

Static density equivalent 0.35 Torr at 297°K

(Note scale difference for the 3^1P and 4^3D lines)

HYD-8361

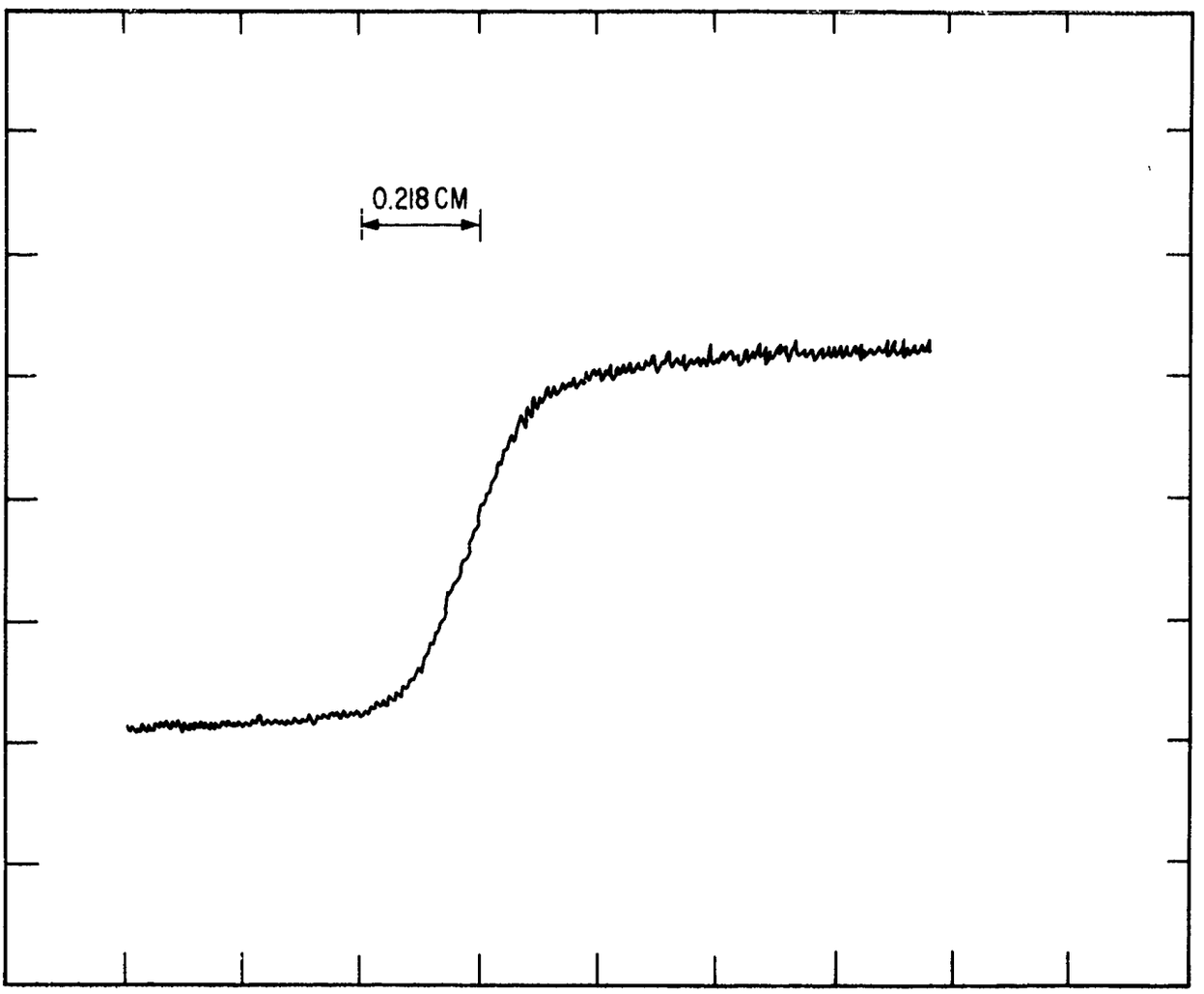

FIG. 3a. SHOCK PROFILE IN NITROGEN. CONTOURED NOZZLE, $M_1 = 1.77$, $p_o = 0.356$ Torr, 3×10^{-7} A full scale. Beam 30 kV at 2 mA.

HYD-8362

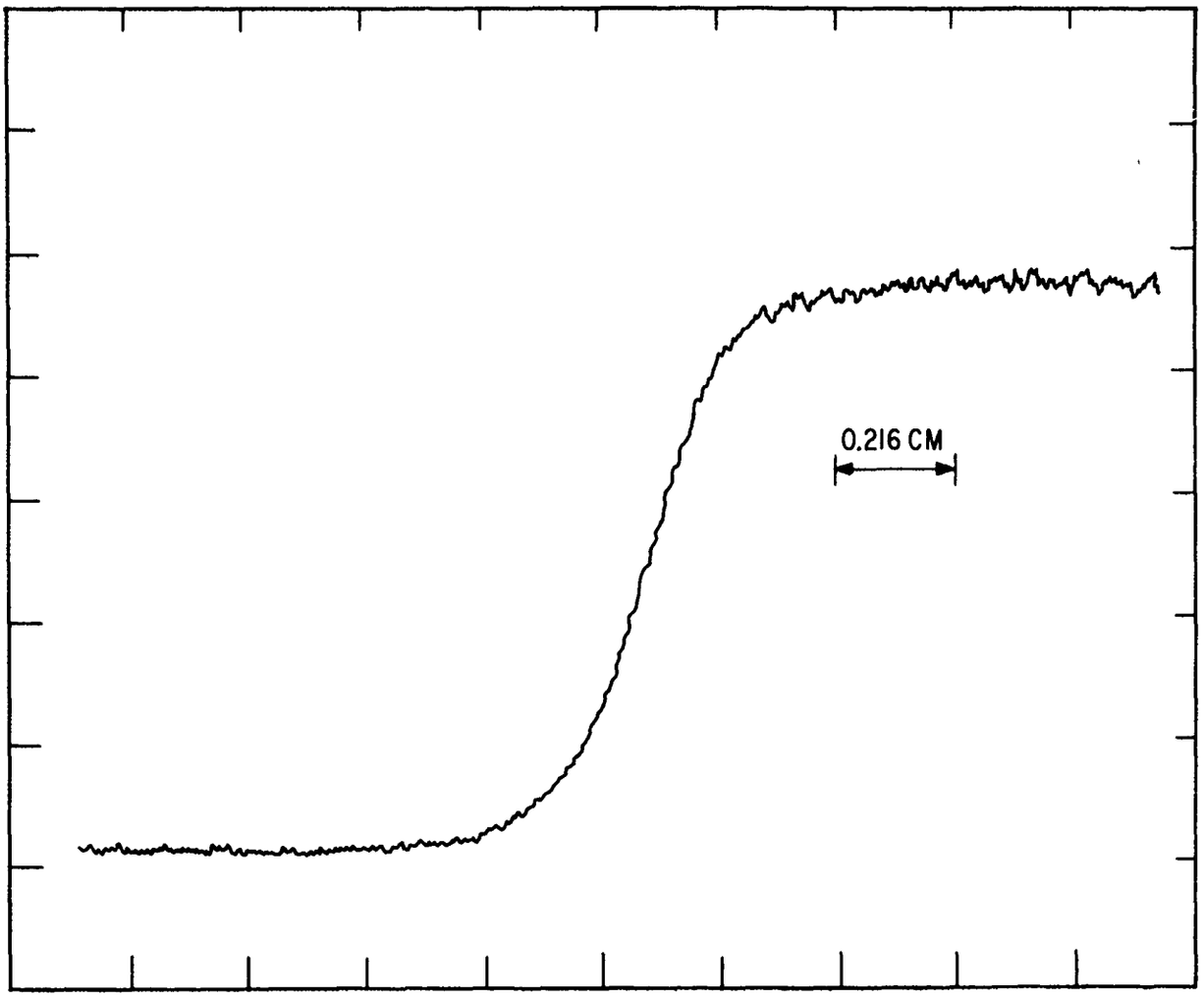

FIG. 3b. SHOCK PROFILE IN NITROGEN. FREE JET, $M_1 = 9.45$, $P_o = 42.0$ Torr, 3×10^{-8} A full scale. Beam 30 kV at 1.5 mA.

HYD-8363

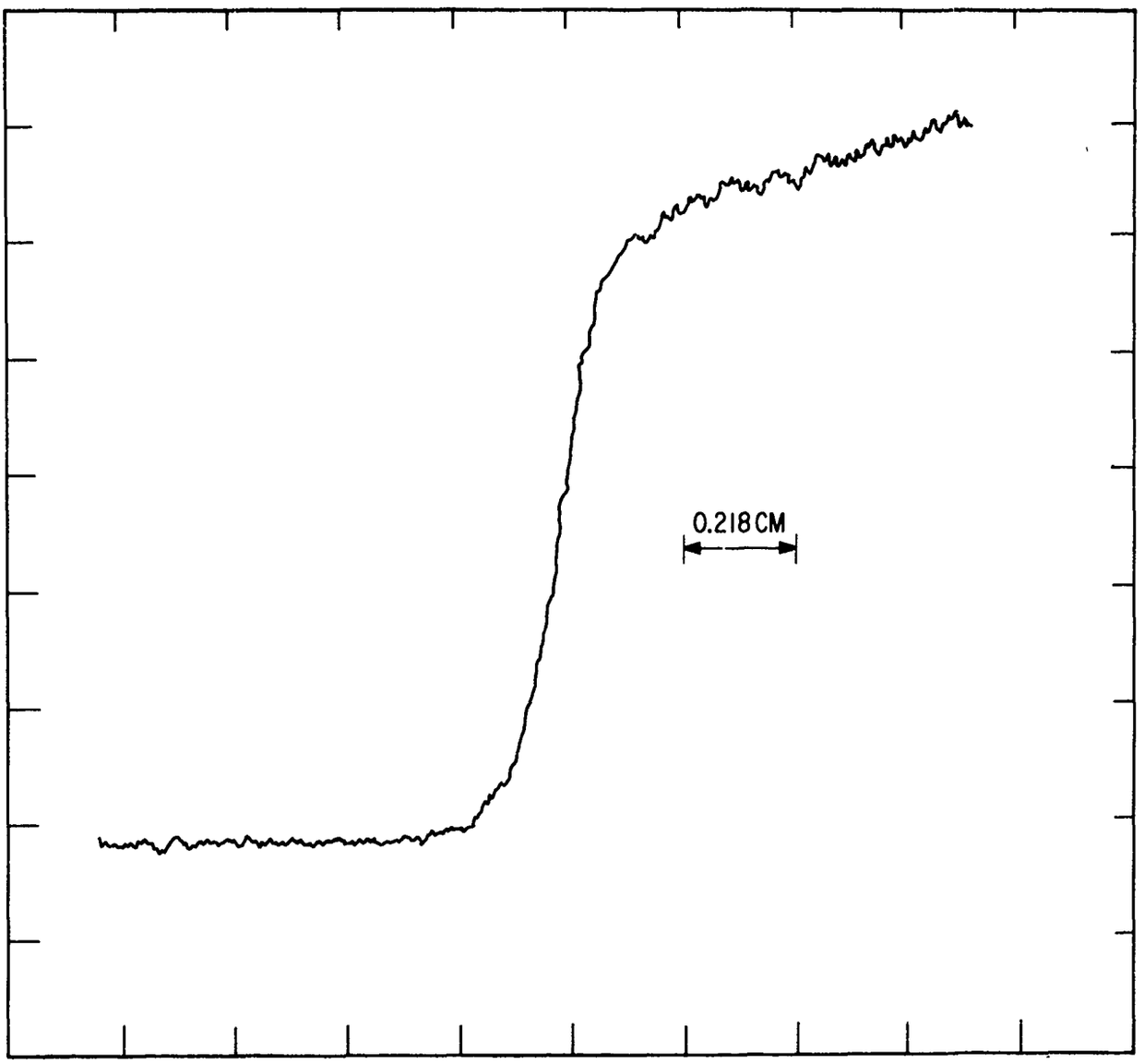

FIG. 3c. SHOCK PROFILE IN ARGON. FREE JET, $M_1 = 17.4$, $p_o = 61.2$ Torr, 3×10^{-9} A full scale. Beam 30 kV at 2.5 mA.

HYD-8364

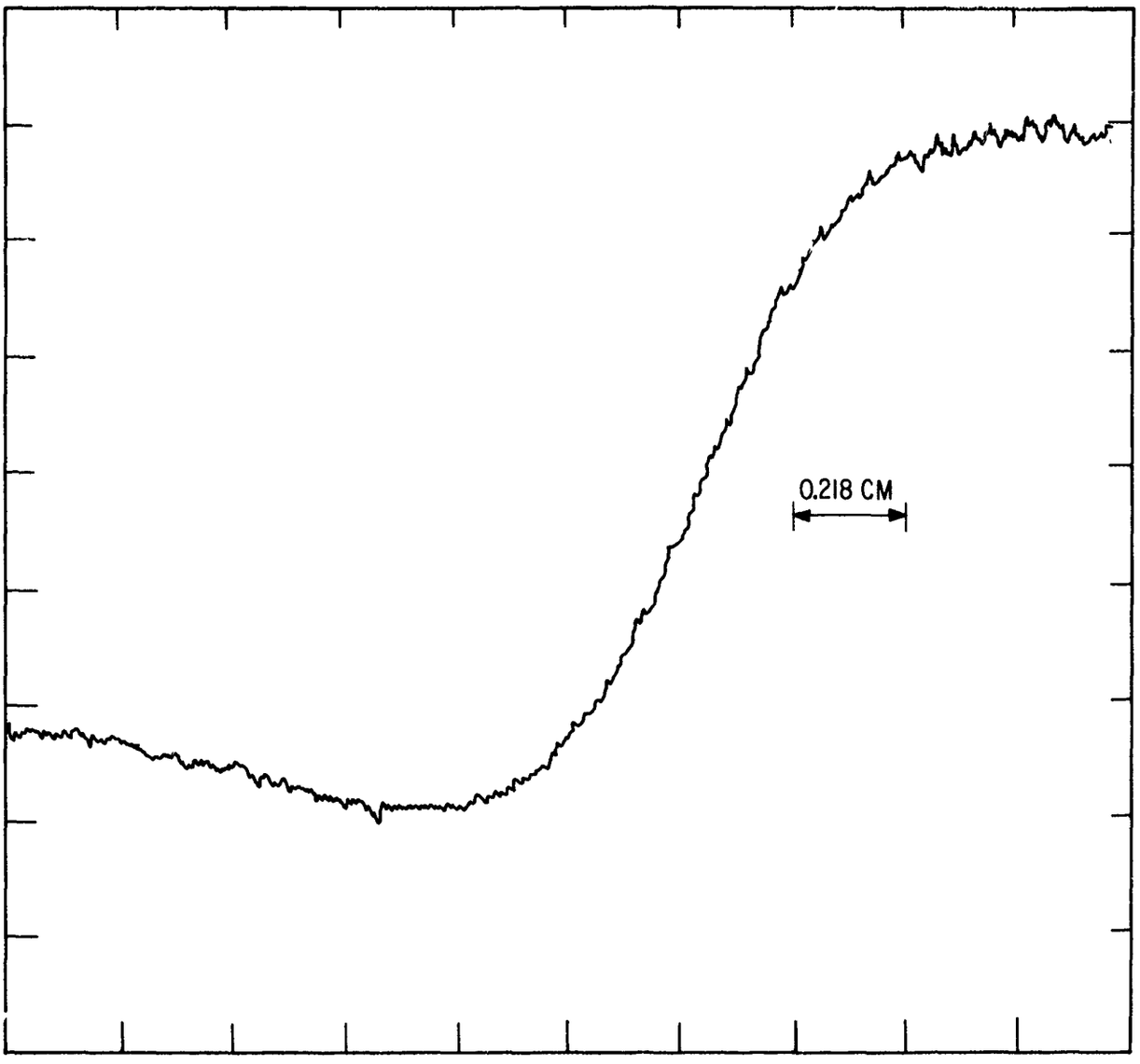

FIG. 3d. SHOCK PROFILE IN HELIUM. FREE JET, $M_1 = 17.4$, $p_o = 51$ Torr, 3×10^{-9} A full scale. Beam 30 kV at 4.0 mA.

HYD-8365

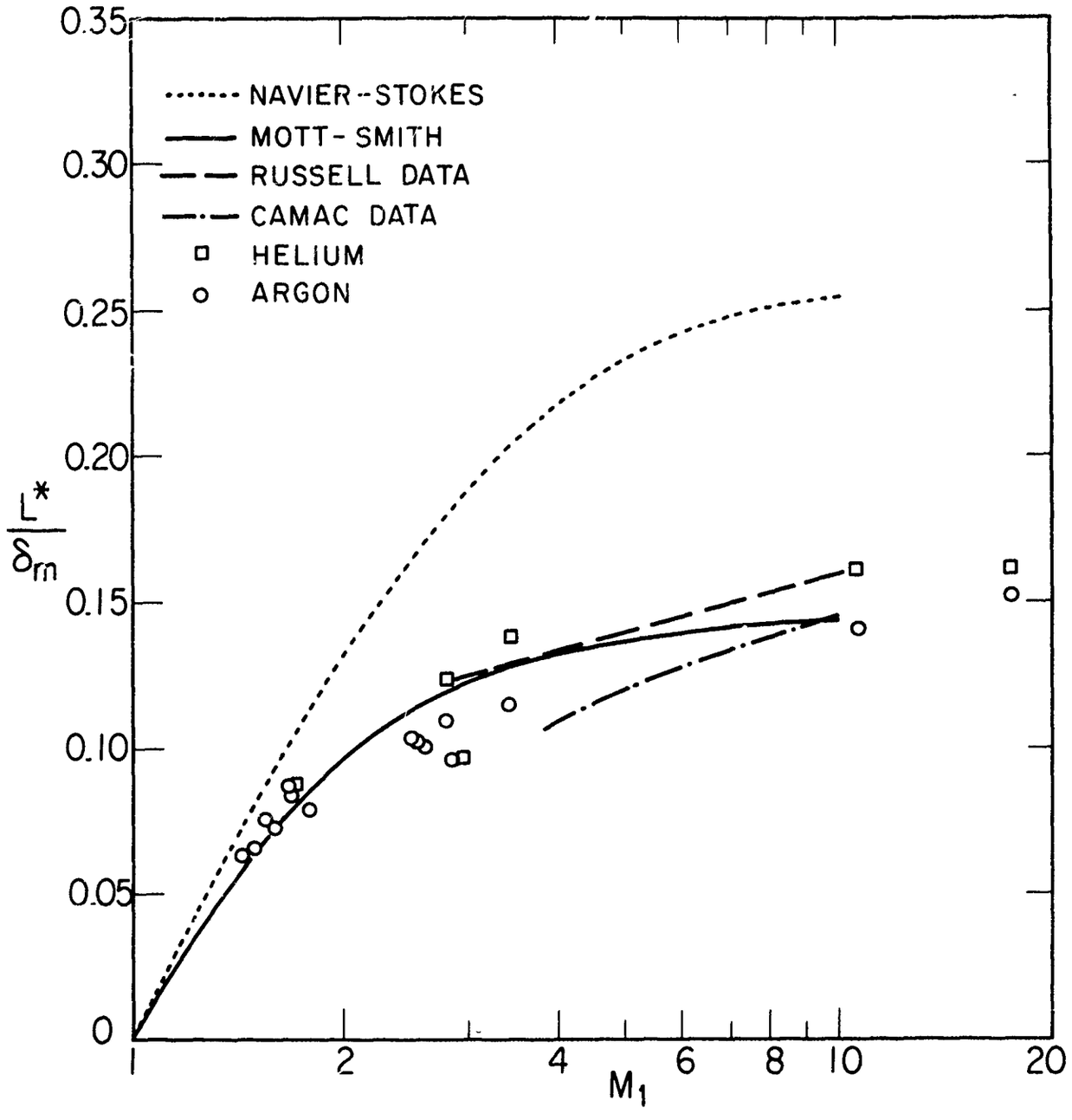

FIG. 4. MAXIMUM-SLOPE THICKNESSES FOR ARGON AND HELIUM

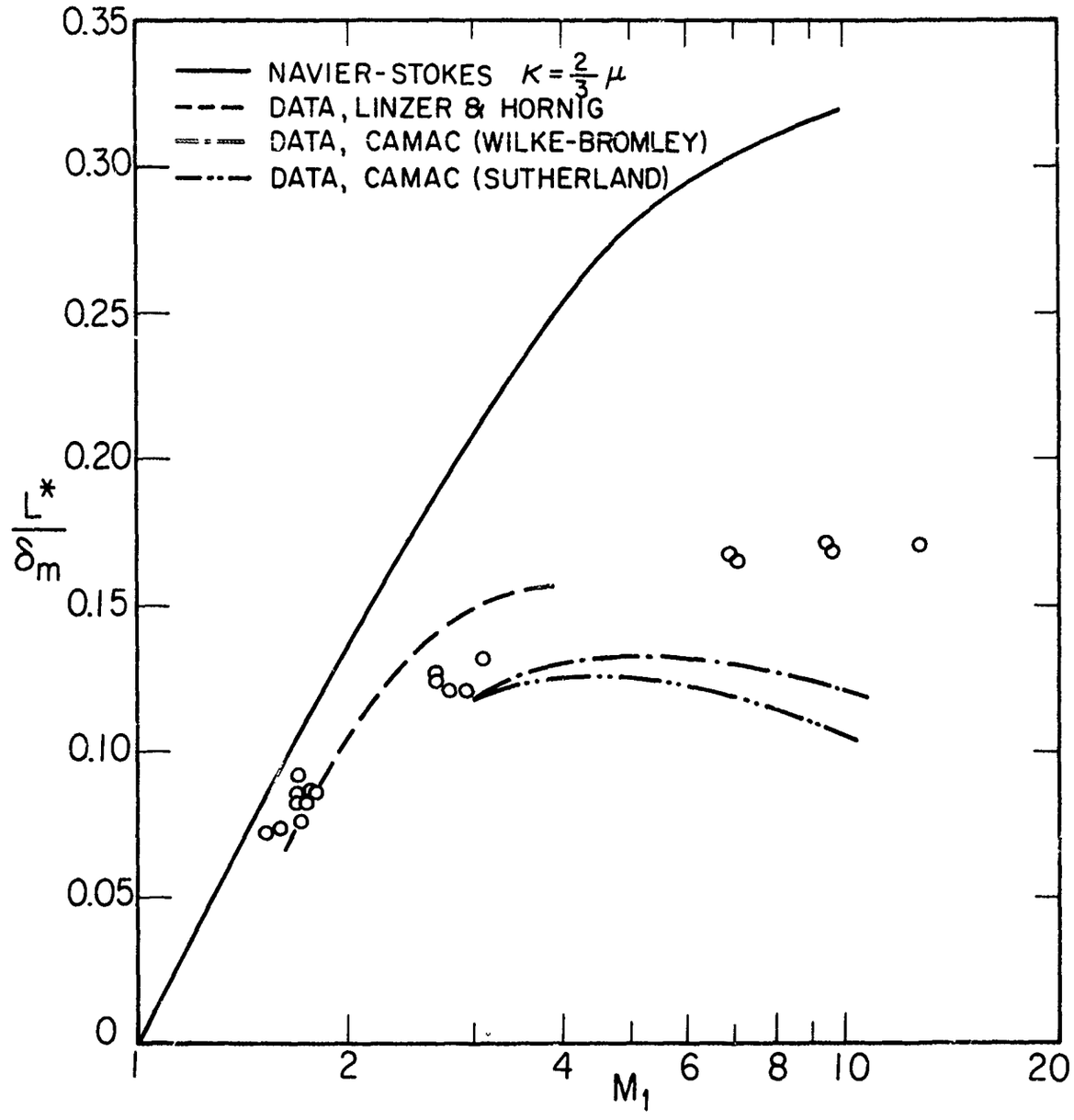

FIG. 5. MAXIMUM SLOPE THICKNESSES FOR NITROGEN

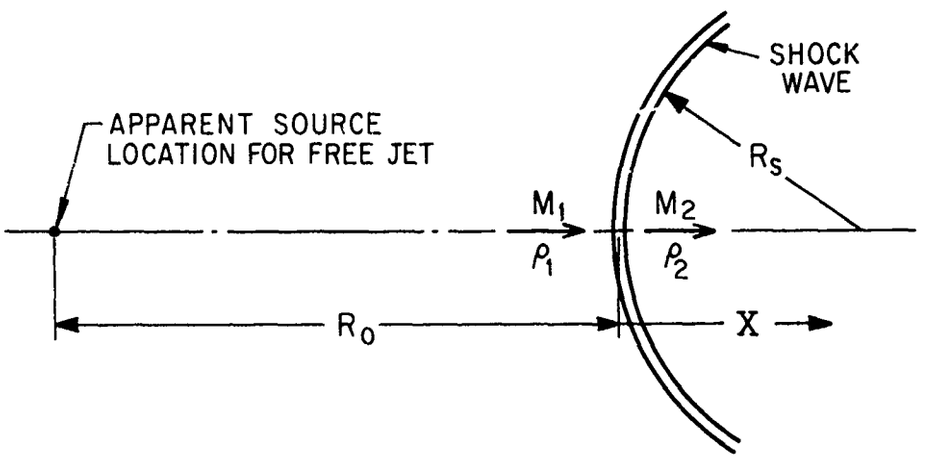

FIG. 6. NOMENCLATURE FOR SHOCK WAVE CURVATURE

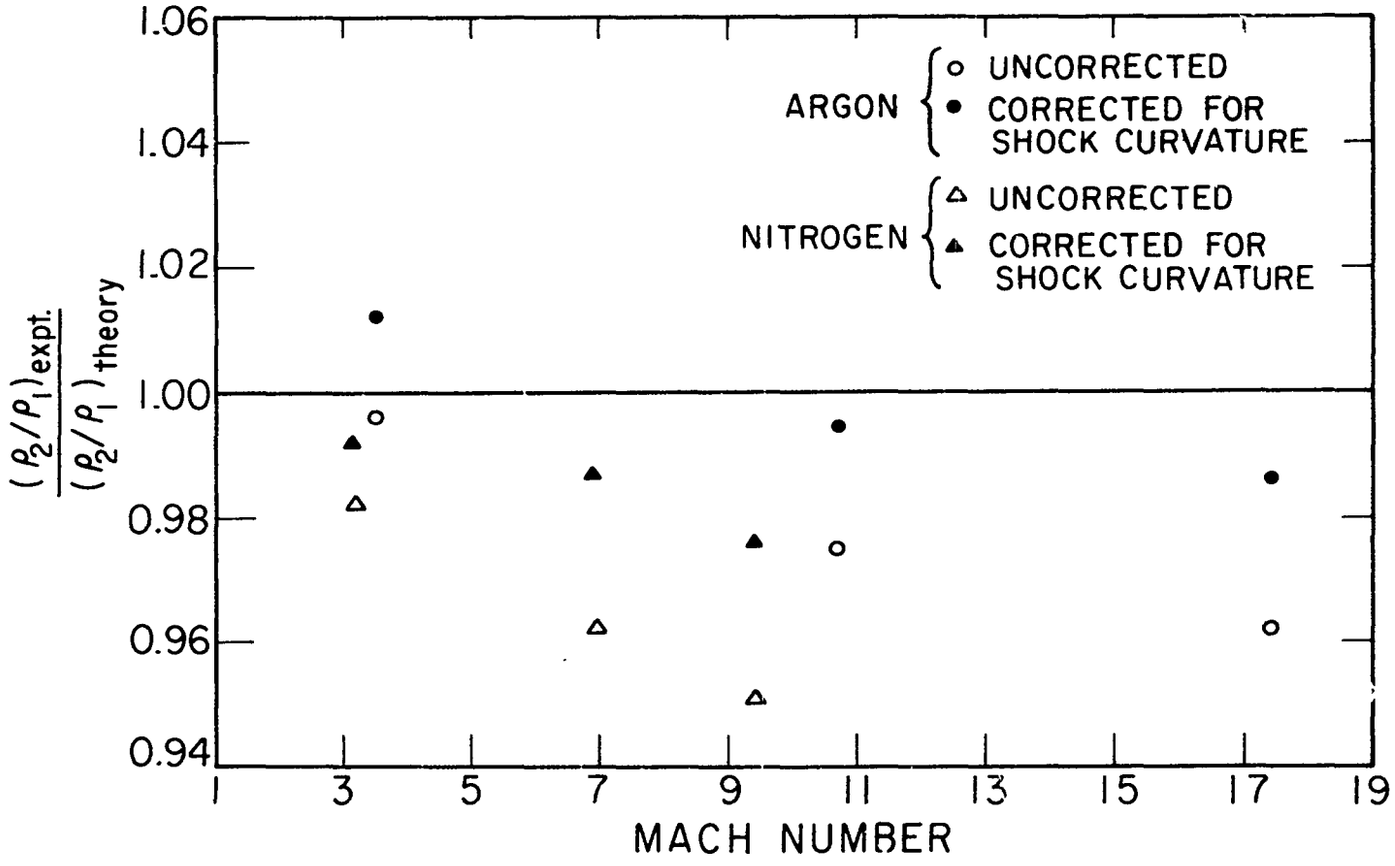

FIG. 7. FREE JET SHOCK WAVE DENSITY RATIOS WITH AND WITHOUT CURVATURE CORRECTIONS

UNCLASSIFIED

Security Classification

DOCUMENT CONTROL DATA - R&D

(Security classification of title, body of abstract and indexing annotation must be entered when the overall report is classified)

1 ORIGINATING ACTIVITY (Corporate author)	2a REPORT SECURITY CLASSIFICATION
University of California, Berkeley	UNCLASSIFIED
	2b GROUP

3 REPORT TITLE

Measurement of Shock Wave Thickness by the Electron Beam Fluorescence Method

4 DESCRIPTIVE NOTES (Type of report and inclusive dates)

Technical Report

5 AUTHOR(S) (Last name, first name, initial)

Robben, F., and Talbot, L.

6 REPORT DATE	7a TOTAL NO OF PAGES	7b NO OF REFS
May 1965	33	27

8a CONTRACT OR GRANT NO	9a ORIGINATOR'S REPORT NUMBER(S)
Nonr-222(45) AFOSR 538-65	AS-65-4
b PROJECT NO	
c	9b OTHER REPORT NO(S) (Any other numbers that may be assigned this report)
d	

10 AVAILABILITY/LIMITATION NOTICES

Qualified requesters may obtain copies of this report from DDC

11 SUPPLEMENTARY NOTES	12 SPONSORING MILITARY ACTIVITY
	Office of Naval Research Air Force Office of Scientific Research Advanced Research Projects Agency

13 ABSTRACT

Shock wave thicknesses and density ratios have been measured in helium, argon and nitrogen by means of the electron beam fluorescence method, over the range $1.5 < M < 17.4$, in a low density wind tunnel. The shock thicknesses in argon and helium agreed well with Mott-Smith theory at the higher Mach numbers, and were between Navier-Stokes and Mott-Smith theory at the lowest Mach number. In nitrogen, the measured shock thicknesses were considerably greater than the predictions of Navier-Stokes theory.

Measured density ratios across the shock wave were in good agreement with theory, in the lower density flows. Poorer agreement was found at higher flow densities, leading to estimates of upper bounds for the range of linear variation of fluorescence intensity with gas density. Measured density ratios for shocks produced in divergent free-jet flows were found to be in better agreement with theory after a viscous curvature correction was applied.

DD FORM 1 JAN 64 1473

UNCLASSIFIED

Security Classification

14. KEY WORDS	LINK A		LINK B		LINK C	
	ROLE	WT	ROLE	WT	ROLE	WT
Rarefied Gas Dynamics Shock Waves Electron beams						

INSTRUCTIONS

1. ORIGINATING ACTIVITY: Enter the name and address of the contractor, subcontractor, grantee, Department of Defense activity or other organization *(corporate author)* issuing the report.

2*a*. REPORT SECURITY CLASSIFICATION: Enter the overall security classification of the report. Indicate whether "Restricted Data" is included. Marking is to be in accordance with appropriate security regulations.

2*b*. GROUP: Automatic downgrading is specified in DoD Directive 5200.10 and Armed Forces Industrial Manual. Enter the group number. Also, when applicable, show that optional markings have been used for Group 3 and Group 4 as authorized.

3. REPORT TITLE: Enter the complete report title in all capital letters. Titles in all cases should be unclassified. If a meaningful title cannot be selected without classification, show title classification in all capitals in parenthesis immediately following the title.

4. DESCRIPTIVE NOTES: If appropriate, enter the type of report, e.g., interim, progress, summary, annual, or final. Give the inclusive dates when a specific reporting period is covered.

5. AUTHOR(S): Enter the name(s) of author(s) as shown on or in the report. Enter last name, first name, middle initial. If military, show rank and branch of service. The name of the principal author is an absolute minimum requirement.

6. REPORT DATE: Enter the date of the report as day, month, year, or month, year. If more than one date appears on the report, use date of publication.

7*a*. TOTAL NUMBER OF PAGES: The total page count should follow normal pagination procedures, i.e., enter the number of pages containing information.

7*b*. NUMBER OF REFERENCES: Enter the total number of references cited in the report.

8*a*. CONTRACT OR GRANT NUMBER: If appropriate, enter the applicable number of the contract or grant under which the report was written.

8*b*, 8*c*, & 8*d*. PROJECT NUMBER: Enter the appropriate military department identification, such as project number, subproject number, system numbers, task number, etc.

9*a*. ORIGINATOR'S REPORT NUMBER(S): Enter the official report number by which the document will be identified and controlled by the originating activity. This number must be unique to this report.

9*b*. OTHER REPORT NUMBER(S): If the report has been assigned any other report numbers *(either by the originator or by the sponsor)*, also enter this number(s).

10. AVAILABILITY/LIMITATION NOTICES: Enter any limitations on further dissemination of the report, other than those imposed by security classification, using standard statements such as:

(1) "Qualified requesters may obtain copies of this report from DDC."

(2) "Foreign announcement and dissemination of this report by DDC is not authorized."

(3) "U. S. Government agencies may obtain copies of this report directly from DDC. Other qualified DDC users shall request through _____."

(4) "U. S. military agencies may obtain copies of this report directly from DDC. Other qualified users shall request through _____."

(5) "All distribution of this report is controlled. Qualified DDC users shall request through _____."

If the report has been furnished to the Office of Technical Services, Department of Commerce, for sale to the public, indicate this fact and enter the price, if known.

11. SUPPLEMENTARY NOTES: Use for additional explanatory notes.

12. SPONSORING MILITARY ACTIVITY: Enter the name of the departmental project office or laboratory sponsoring *(paying for)* the research and development. Include address.

13. ABSTRACT: Enter an abstract giving a brief and factual summary of the document indicative of the report, even though it may also appear elsewhere in the body of the technical report. If additional space is required, a continuation sheet shall be attached.

It is highly desirable that the abstract of classified reports be unclassified. Each paragraph of the abstract shall end with an indication of the military security classification of the information in the paragraph, represented as *(TS), (S), (C), or (U)*.

There is no limitation on the length of the abstract. However, the suggested length is from 150 to 225 words.

14. KEY WORDS: Key words are technically meaningful terms or short phrases that characterize a report and may be used as index entries for cataloging the report. Key words must be selected so that no security classification is required. Identifiers, such as equipment model designation, trade name, military project code name, geographic location, may be used as key words but will be followed by an indication of technical context. The assignment of links, roles, and weights is optional.